Green Analytical Chemistry 5 (2023) 100058

Contents lists available at ScienceDirect

Green Analytical Chemistry

journal homepage: www.elsevier.com/locate/greeac

Rapid extraction and detection of ellagic acid in plant samples using a selective magnetic molecularly imprinted polymer coupled to a fluorescence method

Ouarda El Hani[a,b], Abdelhafid Karrat[a,b], Juan José García-Guzmán[b], José María Palacios-Santander[b,*], Khalid Digua[a], Aziz Amine[a], Laura Cubillana-Aguilera[b]

[a] Laboratory of Process Engineering and Environment, Faculty of Sciences and Techniques, Hassan II University of Casablanca, P.A. 149., Mohammedia, Morocco
[b] Department of Analytical Chemistry, Institute of Research on Electron Microscopy and Materials (IMEYMAT), Faculty of Sciences, Campus de Excelencia Internacional del Mar (CEIMAR), University of Cadiz, Campus Universitario de Puerto Real, Poligono del Río San Pedro S/N, 11510, Puerto Real, Cádiz, Spain

ARTICLE INFO

Keywords:
Magnetic molecularly imprinted polymer
Ellagic acid
Central composite design
Solid-phase extraction
Fluorescence detection
Smartphone detection

ABSTRACT

A remarkable growth was noticed in the development of molecularly imprinted polymers (MIPs), which have used as efficient synthetic antibodies that contain selective cavities to the target molecule. Hereunder, a novel strategy using MIP as a sorbent in solid-phase extraction was coupled to a fluorescence method for ellagic acid (EA) purification and immediate detection. The synthesis of magnetic-MIP (MMIP) using a rapid and green ultrasound technology was assessed by central composite design to determine the optimal polymerization conditions for a high-imprinting polymer. The MMIP was characterized by Fourier transform infrared spectroscopy, X-ray diffraction, thermogravimetric analysis, and scanning/transmission electron microscopy, which accurately confirmed the functional, magnetic, and morphological features of MMIP. The prepared MMIP was demonstrated to be selective for EA compared to many similar phenols. The spectrofluorometric method showed a linear range from 0.05 to 2 $\mu g{\cdot}mL^{-1}$ of EA, and the limits of detection (LOD) and quantification (LOQ) were 0.005 and 0.02 $\mu g{\cdot}mL^{-1}$, respectively. Besides, the novel proposed smartphone method using the ultraviolet lamp as the excitation source presented a linear range from 0.2 to 4 $\mu g{\cdot}mL^{-1}$, a LOQ of 0.2 $\mu g{\cdot}mL^{-1}$, and a LOD of 0.07 $\mu g.mL^{-1}$. The proposed strategy revealed high efficiency in the extraction and detection of EA in grape, redberry, and green tea. Effectively, the calculated recoveries were ranging from 80 to 102% with low values of relative standard deviation (<3%). The proposed strategy could be used in many analytical fields for selective, rapid, user-friendly, visual, and cost-effective detection.

1. Introduction

Typically, a considerable body of literature supports the idea that polyphenols are the best natural sources of various pharmaceutical drugs, and are widely regarded as complementary and alternative remedies that can reduce the danger of many serious diseases (particularly cardiovascular, respiratory, digestive, skin, and cancers), as well as promote them as protective agents [1–4]. Consequently, the extraction of these highly valuable compounds from different aromatic and medicinal plants has moved at the vanguard of search in the medicine field [5]. In this sense, ellagic acid (EA ($C_{14}H_6O_8$)) is a naturally occurring orthodiphenol found in a wide range of plant species [6,7], especially in fruits, particularly pomegranate, grapes, persimmons, raspberries, strawberries, and peaches; moreover, it is also present in seeds like walnuts and almond, along with some tea plants [8,9]. EA is an incredibly interesting compound that has contributed positively to many health aspects due to its properties of interest [10,11], including anti-oxidant [12], anti-inflammatory [13], potential neuroprotective agent [14,15], hepatoprotective [16,17], cytotoxic [18], antitumor, anticancer, and skin protective [19,20]. Therefore, its utilization has been recently promptly popularized.

For this purpose, various extraction approaches have been employed to extract EA from plant matrix [21]. These include Soxhlet extraction [22], liquid-liquid extraction [23], recrystallization [24,25], capillary electrophoresis [26], chromatography [27,28], ultrasonic extraction [29], and microwave-assisted extraction [30]. Nonetheless, the existing methodologies provide many challenges and limitations. They need enormous amounts of solvents and are time consuming. Besides, some of them requires complex instrumentation [31,32]. Moreover, whereas the solid-phase extraction (SPE) method has been extensively

* Corresponding author.
E-mail address: josem.palacios@uca.es (J.M. Palacios-Santander).

https://doi.org/10.1016/j.greeac.2023.100058
Received 13 March 2023; Received in revised form 26 April 2023; Accepted 2 May 2023

applied for EA extraction, it has been reported to have limited selectivity, and purifying efficiency [33]. As a result, the current evidence put its focus on improving the selectivity yield and shortening the extraction procedure. For the same goal, artificial antibodies known as molecularly imprinted polymers (MIPs) [34–36] have been reported to be employed as sorbents in SPE for the efficient isolation and extraction of EA [37,38] owing to their unique advantages, especially the high selectivity, efficiency, and cost-effectiveness [39,40]. Additionally, combining MIP with SPE has been deemed more eco-friendly than conventional SPE, thanks to the use of low volumes of solvents. Magnetic nanoparticles are highly recommended for use in MIPs preparation as core materials, especially that their presence would bypass the filtration and centrifugation standard SPE steps by separating the adsorbent from the bulk sample easily and rapidly using a magnet [41,42]. Concerning the analytical detection of EA, chromatography [43] and fluorescence [44,45] are the commonly used methods. Furthermore, the smartphone detection became recently a highly recommended tool in food assessment compared to many laboratory methods owing to its portability, simplicity, rapidity, low-cost, and eco-friendliness [46]. For this reason, the smartphone-based fluorescence detection of EA is considered a promising sensing technique for the on-site rapid detection. To the best of our knowledge, this method was used for EA for the first time in this work. MIP synthesis was highly recommended to be examined by response surface methodologies, particularly central composite design (CCD), Box-Behnken, and Doehlert to assess the influential factors on MIP preparation and to determine the most adequate experimental conditions for a rapid and relevant polymerization. Indeed, CCD is the widely utilized experimental design because it can fit a complete quadratic model and involve sequential experimentation [47,48].

In the current work, a new magnetic-MIP (MMIP) for EA was ultrasonically prepared by an optimized radical green polymerization using the CCD approach. The synthesized MMIP revealed strong affinity towards EA compared to several similar phenols. Fourier transform infrared spectroscopy, X-ray diffraction, thermogravimetric analysis, and scanning/transmission electron microscopy were used to define the functional, morphological and textural characteristics of the developed imprinting polymer. Subsequently, the MMIP was successfully applied in SPE for the quick, ecofriendly, and selective extraction of EA. The developed MMIP-SPE was coupled to a fluorescence method for accurate and precise detection of EA in grape, redberry, and green tea samples. Moreover, smartphone-based fluorescence detection was effectively applied for a rapid, cheap, and on-site detection of EA in these samples. The smartphone-based fluorescence method for EA sensing was reported for the first time in this work. Moreover, the optimization by applying the CCD plan enhanced the MMIP performance in SPE methodology.

2. Experimental study

2.1. Reagents

EA ≥97%, ferric chloride hexahydrate ($FeCl_3{\cdot}6H_2O$) ≥98%, ferrous chloride tetrahydrate ($FeCl_2{\cdot}4H_2O$) 99%, ammonium hydroxide (NH_4OH), oleic acid (OA), sodium dodecyl sulfate (SDS) ≥99%, methacrylic acid (MAA) 90%, ethylene glycol dimethacrylate (EGDMA) 98%, ammonium persulfate (APS) ≥98%, sodium hydroxide (NaOH), borax ($Na_2B_4O_7{\cdot}10H_2O$) ≥99%, gallic acid (GA) ≥98%, caffeic acid (CA) ≥98%, catechol ≥99%, ferulic acid (FA) 99% and β-estradiol ≥98% were purchased from sigma Aldrich (Spain). Dimethyl sulfoxide (DMSO) >99% and methanol 99.9% were purchased from PanReac (Spain). Distilled water (18 MΩ cm) was obtained from a Millipore Milli-Q system (Bedford, MA, USA).

2.2. Instrumentation and apparatus

A high-power ultrasound probe SONICATOR 4000 (Misonix Inc., Farmingdale, NY, USA), operating at 20 KHz, with a maximum output power of 700 W and equipped with a titanium tip of 13-mm diameter, was used in the MMIP synthesis. Fourier transform infrared (FT-IR) spectra of the materials were collected using an Affinity-1S IR spectrophotometer (Shimadzu, Japan), in attenuated total reflectance (ATR) mode and in a range of 4000–500 cm^{-1}, to assess the functional characteristics of the developed MMIP and magnetic nanoparticles (MNP). X-ray diffraction (XRD) measurements were recorded on a Bruker D8 Advance A25 X-ray diffractometer (BRUKER-AXS, Germany), equipped with a LINXEYE detector, a Cu-Kα radiation source (λ=0.1542 nm), and a 2θ step of 0.02035 was employed to define the composition of the developed materials. Thermo-gravimetric analyses (TGA) were performed on a TGA Q50 V20.13 Build 39 from TA Instruments (Delaware, USA) by heating from 30 to 800 °C at a rate of 10 °C/min under nitrogen:air flow (4:6 v/v). The double beam Scios2 electron microscope (Thermo Fisher Scientific, USA), operating in scanning/transmission (STEM) mode was employed to obtain the STEM images of MMIP and MNP. Finally, an FP-6500 spectrofluorometer (Jasco, Spain) was used for EA determination.

2.3. Synthesis of modified MNP

2.3.1. Preparation of MNP

According to Messaoud et al. [49], MNP were synthesized as follows. Firstly, 13.56 g of $FeCl_3{\cdot}6H_2O$ and 4.96 g of $FeCl_2{\cdot}4H_2O$ were dissolved with 250 mL of Milli-Q water in a flask under nitrogen deoxygenation (N_2). In the second step, 20 mL of NH_4OH was added while being vigorously and continuously stirred for 40 min at 80 °C. Finally, the synthesized nanoparticles were washed with Milli-Q water to eliminate any undesired elements. The collected material was dried at 50 °C.

2.3.2. Preparation of ferrofluidic solution

As stated by karrat et al. [35], to prepare the aqueous ferrofluidic solution, 100 mg of the previous prepared MNP were dispersed in 10 ml of Milli-Q water under sonication for 5 min at 60 °C. Next, 70 μL of OA and 67 mg of SDS were successively introduced to the aqueous solution under ultrasonic treatment for 10 min.

2.4. Optimization of MMIP synthesis by CCD

In order to develop high-affinity polymers towards target molecules, response surface methodology (RSM) is assumed to become a vital step during the synthesis to select the most suitable polymerization conditions [47]. Many experimental approaches were employed to achieve this goal, particularly the CCD was applied in this study to optimize the effective parameters on the imprinting factor which was calculated for each synthetized MMIP versus its corresponding magnetic non-imprinted polymer (MNIP). The main studied factors (EA amount, added volume of MAA, and the probe amplitude), their symbols (X_1, X_2, and X_3, respectively), and their levels are presented in **Table. S1**. In the CCD plan, 32 experiments were performed randomly (16 runs for MMIP and 16 runs for MNIP) with 2 center points, 8 factorial points, and 6 axial points placed at a distance of α=1.287 from the center as indicated in **Table. S2.**

The measured dependent variable in each run was the imprinting factor (IF), which was calculated based on the uptake capacity Q ($mg{\cdot}g^{-1}$) of MMIP and MNIP as defined by the following equations (Eq. (1) and Eq. (2)):

$$Q\left(\mathrm{mg}\cdot\mathrm{g}^{-1}\right)=\frac{C_i-C_e}{m}\times V \tag{1}$$

Where C_i ($\mu g{\cdot}mL^{-1}$) is the initial concentration of EA; C_e ($\mu g{\cdot}mL^{-1}$) is the equilibrium concentration of EA which was not adsorbed by the polymer; V (mL) is the volume of the adsorption solution; and m (mg) is the mass of MMIP and MNIP.

$$IF=\frac{Q(MMIP)}{Q(MNIP)} \tag{2}$$

Where Q(MMIP) and Q(MNIP) are the amount of EA adsorbed by MMIP and MNIP, respectively. A value of IF >1 confirms the presence of the EA shaped-cavities in the prepared MMIP. The imprinting polymer shows high performance when the IF reaches high values.

2.5. Preparation of MMIP using a high-power ultrasound probe

After defining the optimum conditions of MMIP synthesis using CCD, the optimal procedure of the preparation is detailed below.

Prior to the polymerization synthesis of EA-MMIP, a self-assembly solution was prepared with 20.3 mg of EA as template molecule and 300 μL of MAA as functional monomer, which were dissolved in 30 mL of DMSO:Milli-Q water (2:1) as the porogen solvent. The preceding solution was stored for 1 h at 4 °C to promote the hydrogen bonding interactions between EA and MAA.

The polymerization of EA-MMIP was performed using a high-power ultrasound probe by applying the following procedure. Firstly, the self-assembly solution was added to a beaker glass that contains 20 mL of the prepared dispersed MNP. Secondly, 317 μL of cross-linker EGDMA was added to the blend to link between the poly-MAA chains. Thirdly, 20 mg of APS was introduced to initialize the free radical polymerization. The N_2 gas was purged in the solution for its deoxygenation during 15 min. The previous mixture was left 40 min at 45% of the probe amplitude for the polymerization completion. The formed polymer was washed with NaOH (0.1 M) until the complete template removal. The EA removal was assessed by UV–Vis spectrophotometry (spectrophotometer model T80+ from PG Instruments, Leicestershire, England) at λ=360 nm. Finally, the resultant polymer was washed several times with Milli-Q water to remove any trace of solvents. Same procedure was followed for MNIP synthesis without using the template molecule.

2.6. Binding properties of the developed MMIP

The fundamental challenge in MIPs is proving the effective creation of the imprinting sites. Accordingly, to investigate the binding characteristics of the developed materials, 4 mg of MMIP or MNIP was dispersed in 2 mL of various EA concentrations ranging from 0.1 to 8 $\mu g{\cdot}mL^{-1}$ dissolved in methanol: Milli-Q water (1:1). The prior adsorption solutions were shaken at 600 rpm for 15 min at room temperature (25 °C), followed by the solid-liquid separation of the previous dispersive solutions using a magnet. 100 μL of borax 85 $mg{\cdot}mL^{-1}$ was added to the supernatants and, the mixtures were measured by fluorescence technique at an excitation and emission wavelengths of 383 and 469 nm, respectively. Each experimental point was measured with three replicates.

The isotherm results were assessed to fit the Freundlich and the Langmuir models which are presented in the Eq. (3) and Eq. (4), respectively.

$$Ln\left(Q_e\right) = \frac{1}{n}\ln\left(C_e\right) + \log\left(K_F\right) \tag{3}$$

Where Q_e ($mg{\cdot}g^{-1}$) is the equilibrium adsorption capacity; 1/n is related to the adsorption intensity; and K_F ($mg{\cdot}g^{-1}$) is the Freundlich constant.

$$\frac{C_e}{Q_e} = \frac{1}{Q_m}C_e + \frac{1}{Q_m K_L} \tag{4}$$

Where Q_m ($mg{\cdot}g^{-1}$) is the maximum uptake concentration; K_L ($L{\cdot}mg^{-1}$) is the Langmuir constant; and C_e ($\mu g{\cdot}mL^{-1}$) is the equilibrium EA concentration.

Likewise, five EA analogue molecules, notably GA, CA, catechol, FA, and β-estradiol were evaluated in the selectivity investigation. Thereupon, 2 ml of 5 $\mu g{\cdot}mL^{-1}$ of each tested molecule was dissolved in methanol: Milli-Q water (1:1). 4 mg of MMIP or MNIP was added. The solution was mixed at 600 rpm for 15 min. The supernatant was obtained after the separation by the magnet. In the detection step, 100 μL of borax (85 $mg{\cdot}mL^{-1}$) was added to each supernatant, which was further analyzed using the spectrofluorometer at the specific excitation and emission wavelengths of each molecule, as outlined below: EA (λ_{ex}=383 nm, λ_{em}=469 nm), GA (λ_{ex}=280 nm, λ_{em}=360 nm), CA (λ_{ex}=365 nm, λ_{em}=450 nm), catechol (λ_{ex}=340 nm, λ_{em}=370 nm), FA (λ_{ex}=340 nm, λ_{em}=400 nm), and β-estradiol (λ_{ex}= 290 nm, λ_{em}= 365 nm). For each phenol, a factor of selectivity (α) was calculated by the following expression (Eq. (5)):

$$\alpha = \frac{Q(EA)}{Q(analogue\ molecule)} \tag{5}$$

Where Q (EA) and Q (analogue molecule) were the uptake capacities of MMIP towards EA and the analogue molecule, respectively. A value of α>>1 confirms the effective selectivity of the prepared MMIP towards EA.

2.7. Application of MMIP as a sorbent in SPE

The developed EA-MMIP was further employed as a sorbent material in SPE study by following the procedure illustrated in Scheme (A). 2 mL of EA aqueous solution was added to 4 mg of MMIP, and the solution was shaken for 15 min to enable the selective binding of EA on its specific shaped cavities located in the MMIP. Next, the supernatant was separated from the material using a magnet. The obtained MMIP was eluted with 2 mL of the methanol: Milli-Q water (1:1). The mixture was shaken for 15 min. Finally, the obtained supernatant was measured by the spectrofluorometer.

2.8. Detection of EA

2.8.1. Fluorometric detection of EA

The presence of borax with EA promoted the formation of a fluorescent complex between the o-dihydroxy groups of EA and borax. The binary complex is excited and emitted at 383 and 469 nm of wavelengths, respectively. The detection method was reported in the following work [45] as detailed briefly in the subsequent protocol. First, 100 μL of borax (85 $mg{\cdot}mL^{-1}$) was added to 2 mL of an EA concentration which was dissolved in methanol: Milli-Q water (1:1). The mixture was immediately measured using the spectrofluorometer in the corresponding wavelengths (λ_{ex}=383 nm and λ_{em}=469 nm). As well as, the previous solution was measured using a handheld ultraviolet lamp (UV lamp) as the excitation source (λ_{ex} around 395 nm) and the smartphone as the readout tool of the emitted light in a perpendicular direction. The fluorescence signal was analyzed by free ImageJ software to assess the RGB values and to construct furtherly the calibration curve of the on-site detection of EA as depicted in Scheme (B).

2.8.2. Determination of EA in real samples

The developed strategy MMIP-SPE associated with the spectrofluorometer and smartphone-based fluorescence for the extraction and determination of EA in natural fruit juices (grape and redberry) and green tea is detailed below.

Using the borax reagent, the initial concentration found in real samples was measured. The samples were spiked with 0.5 and 1 $\mu g{\cdot}mL^{-1}$ of EA. After that, 4 mg of MMIP was added to 2 mL of the sample and was shaken for 15 min. After the separation step, the uptake concentration of EA by the MMIP was eluted in 2 mL of methanol: Milli-Q water (1:1) under stirring for 15 min. Finally, the mixture was fluorometrically measured. Based on the experimental results, the recoveries and relative standard deviation were calculated to evaluate the accuracy and the precision of the strategy.

3. Results and discussion

3.1. CCD optimal conditions for MMIP preparation

The quality of the applied quadratic model was assessed by ANOVA (as detailed in **Table. S3**). The important value of determination coefficient (R^2=0.953) and the significant observed value of the mathematic

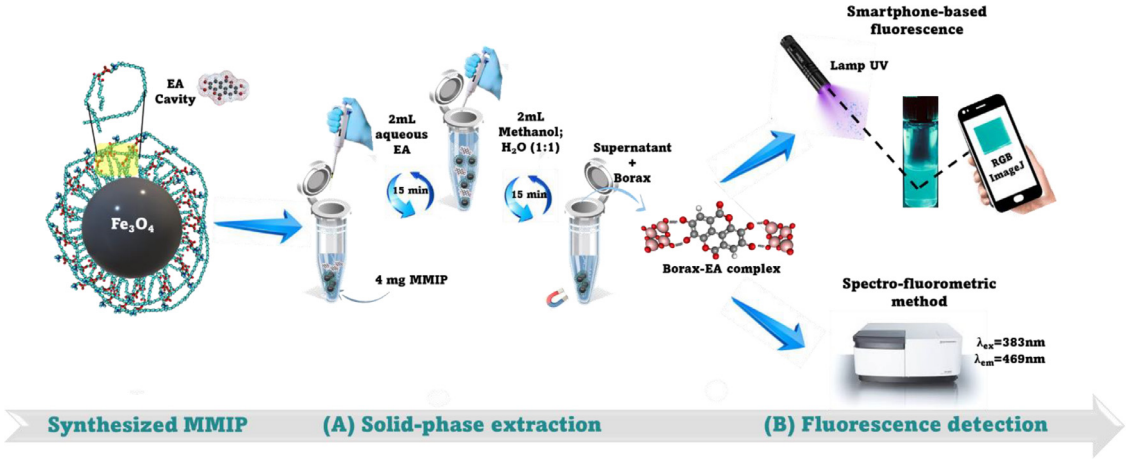

Scheme. Illustration about the fast and selective extraction of EA using MNP in SPE, followed by fluorescence detection.

model (P-value=0.0024<0.05%) implied that the CCD model had a satisfactory goodness of fit between the experimental and the predicted values. In addition, it was found that 88.3% of the data was well explained by the model (R_{adj}^2=0.883). Moreover, the lack-of-fit was revealed to be insignificant (P-value>0.05), which describes the relevant relationship between the experimental variables and the response (IF). Furthermore, X_3 (Probe amplitude), the quadratic term of X_1 (MIP amount^2), and X_3 (Probe amplitude^2) were the critical factors in the variation of the imprinting factor (P-values << 0.05). The significant effect of the quadratic terms of X_1 and X_3 implied that the surface response plot had a curvature form (concave) in terms of X_1 and X_3 variation.

The equation below (Eq. (6)) described the relationship between the influential variables and the imprinting factor (IF).

$$IF = 2.779 - 0.343\ X_3 - 0.713\ X_1^2 - 0.765\ X_3^2 \quad (6)$$

The three dimensional response profile (illustrated in Fig. 1) represented the curvature variation of the imprinting factor of the prepared MMIP depending on the used EA amount in the self-assembly and the employed probe amplitude during the polymerization, while fixing the volume of the monomer (MAA) in 300 μL. The desirable experimental regions corresponded to the top-curvature areas which were colored in purple.

As shown in the predictor profiler illustrated in **Fig. S1A**, EA amount (X_1) has a slight influence in the imprinting factor variation. However, it should be mentioned that employing very small amounts of EA (≤8 mg) in the MMIP synthesis led to the formation of relative weak imprinting polymer (IF=1.5) due to the insufficient quantity of the template that normally interacted with the functional monomer to form the specific cavities of EA during the self-assembly step. Moreover, same conclusion was remarked in the case of using very high amount of EA (≥30 mg). When EA is plentifully employed in the synthesis, the rest of EA that did not react with the monomer in the self-assembly step, can be involved in the reaction with APS. As a result, the radical polymerization would not be perfectly carried out, similarly the yield of the polymerization could be reduced as well. Nevertheless, medium amount of EA was the most adequate for the synthesis to overcome the previous difficulties. Thus, 20.3 mg was the recommended amount based on the maximization of the desirability function of the CCD model. Concerning the volume of the monomer, it is quite clear that it had non-significant influence on the imprinting factor variation, but to maximize the response, it was fixed at 300 μL as shown in **Fig. S1B.**

Moreover, it should be noted from the **Fig. S1C** that high amplitudes of the probe (such as 70%) corresponded to the low imprinting values (IF=1), which can be justified by the possibility of the destruction of the EA shaped cavities when using very strong powers in the synthesis. Besides, low imprinting factors characterized the synthesized MMIPs with very low amplitudes (such as 28%), and this can be due to insufficient cavities formed in the corresponding polymers. In this case, higher energy and prolonged synthesis times will be required. Nonetheless, the medium amplitudes of the probe exhibited the highest binding capacities and also great polymer yields, which can be justified by considering that these moderate powers led to a sufficient energy release, enhancing the cavitation intensity and, consequently, increasing the yield of the polymerization without destroying the polymer functions.

To recapitulate, the optimum conditions of the MMIP preparation were fixed in the following optimal setting: X_1 = 20.3 mg; X_2 = 300 μL; X_3 = 45%; IF = [2.6; 3.4]; Desirability = 0.89, while maximizing the desirability function.

3.2. Green aspects of the developed methodology

The actual research trends are emphasized in the development of green and rapid preparation protocols. Actually, the MMIP preparation method is environmentally friendly and rapid, since, instead of using toxic organic solvents, DMSO, which is less dangerous due to its biodegradability, high boiling point, and low vapor pressure, was employed with a reduced volume in the MMIP synthesis. Besides, the APS was used to initialize the radical polymerization due to its low toxicity compared with other initiators such as azobisisobutyronitrile. Also, APS is preferably used owing to its high solubility in water. Furthermore, to the best of our knowledge, the reduced time for the EA imprinting polymers polymerization was achieved for the first time for EA imprinting analysis in the present work. Furthermore, the moderate applied amplitude during the synthesis reinforced the green aspect of this method.

Protocol of EA extraction and detection in fruit samples was evaluated using a greenness approach called AGREE, which is based on 12 green analytical chemistry (GAC) principles as detailed in the following works [50,51]. The green score of each principle was ranging from 0 to 1 depending on the agreement of the evaluated protocol with the GAC principle. Scoring results of the 12 principles, which were applied for EA sensing protocol, were detailed in **Table. S4**. Clock-like AGREE graph of the three color representation (green-yellow-red scale reflected the high-medium-low GAC accordance) was illustrated in **Fig. S2**. The reported EA sensing method represented efficient green aspects of an average greenness score equal to 0.71.

3.3. Characterizations of MNP and MMIP

Several characterization techniques were employed for the studied materials. The FT-IR spectra of MNP and MMIP (Fig. 2A) demonstrated the presence of the Fe-O functional group at 549 cm^{-1} in both spectra (for MMIP and MNIP), what demonstrated the decoration of MMIP

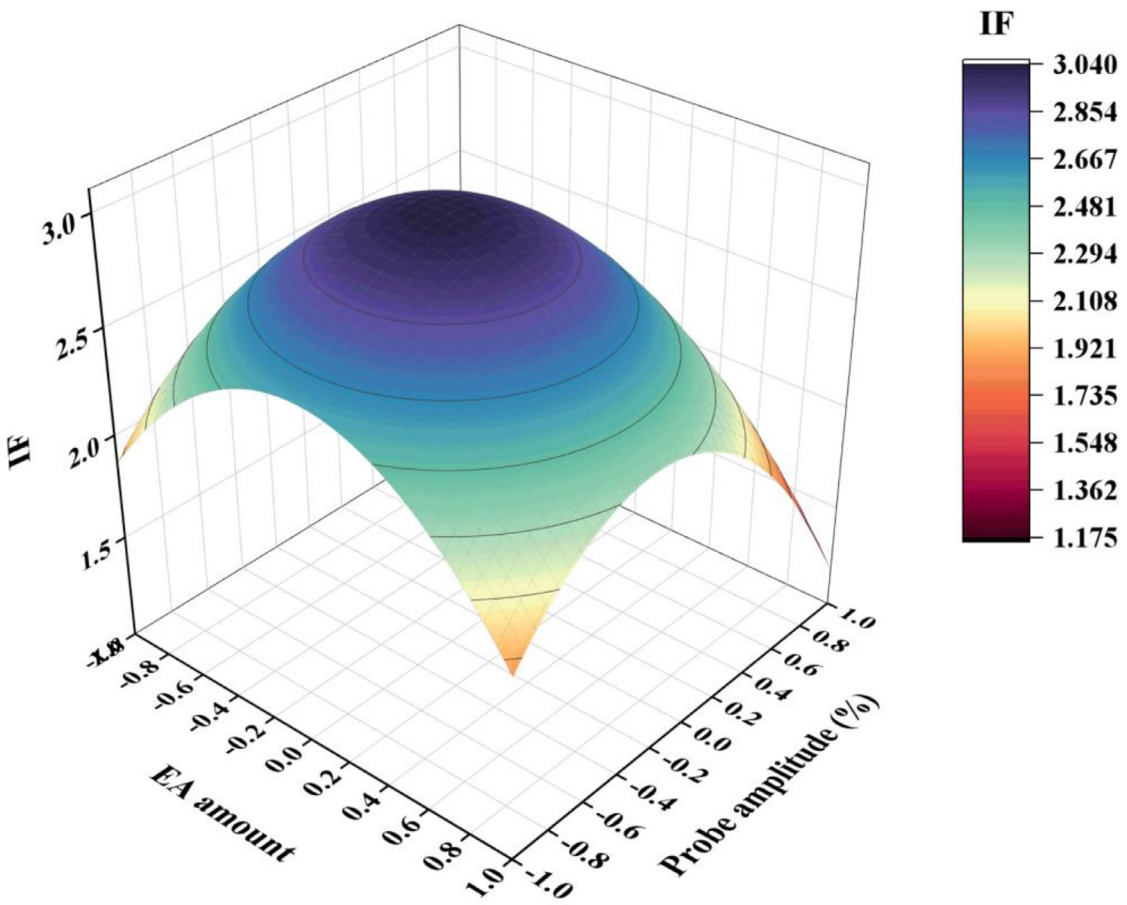

Fig. 1. 3D surface response plot of the imprinting factor in terms of EA amount and the probe amplitude, while fixing MAA volume at 300 μL.

with MNP. In addition, the MMIP spectrum is characterized for the presence of the polymethacrylic peaks at 1726 cm^{-1} and 1157 cm^{-1}, which corresponded to C = O and C–O functional groups, respectively, demonstrating the successful preparation of the polymer.

The same materials were characterized by XRD as shown in Fig. 2B. This figure presented he XRD spectra of MNP and MMIP. Both were characterized for the presence of six typical peaks of MNP at 2θ values of 30^0, 35^0, 43^0, 53^0, 57^0, and 62^0 that are related to the following planes (2 2 0), (3 1 1), (4 0 0), (4 2 2), (5 1 1), and (4 4 0), respectively. Thus, confirming the magnetic composition of the developed MMIP (core of the material).

The findings of TGA displayed in Fig. 2C proved the thermal stability of the synthesized MMIP. The thermograms of MNP and MMIP showed a weight decrease when raising temperature from 250 to 450 ^{0}C, with a loss of 2% and 66%, respectively. The vital weight loss is seen with MMIP due to the decomposition of the polymer around the MNP, suggesting the effective encapsulation of MNP by the imprinted polymer. Yet, no noticeable weight loss was found beyond 450 ^{0}C, indicating that only the thermal-resistant MNPs were left.

STEM technique was adopted to provide the crucial morphology of MNP and MMIP. Fig. 2D illustrated the STEM image of the employed magnetic nanoparticles in spheric forms with a diameter of 10±1.45 nm (n = 16). Nevertheless, the STEM image of MMIP presented in Fig. 2E showed some network morphology remarked with the presence of MNP clusters surrounded by polymeric cover, which demonstrated the decoration of the imprinted polymer by MNPs.

3.4. Adsorption isotherm

The isotherm evaluation of MMIP and MNIP has yielded a better understanding of the affinity distribution features of the developed imprinted polymer. Fig. 3A illustrated the isotherm study for MMIP and MNIP. The figure showed that the uptake capacities of MMIP and MNIP were increased in terms of EA concentration. Moreover, the adsorption capacities of MMIP were always higher than the capacities of MNIP. This fact means that the MMIP contained specific cavities to EA. This result was confirmed by the important value of the imprinting factor (IF=3).

The isotherm data was fitted to Freundlich and Langmuir binding models. **Fig. S3** showed that the isotherm results fitted better with Freundlich (R^2 (MMIP)=0.997, R^2 (MNIP)=0.994) versus Langmuir model (R^2(MMIP)=0.891, R^2(MNIP)=0.868) (as presented in **Table. S5**). These findings means that MMIP revealed a multi-molecular layer adsorption properties. **Table. S6** summarized the calculated Freundlich parameters confirming the affinity of the MMIP towards the EA (n (MMIP)=1.6 > n (MNIP)=0.7 and K_F (MMIP)=5.2 > K_F (MNIP)=0.03).

3.5. Selectivity study

The selectivity study was carried out against several related phenolic compounds to EA. The main reason to choose them is because they are the main compounds detectable by fluorescence method using borax, and some of them (gallic acid, caffeic acid, catechol, and ferulic acid) are considered as the most common phenols found with EA in fruit samples. The Fig. 3B and **Table.S6** revealed that the uptake capacities of MMIP towards EA were found to be significantly higher than towards GA, CA, catechol, FA, and β-estradiol. Moreover, the difference between Q (MIP) and Q (NIP) was not significant for the analogous compounds. Furthermore, MMIP revealed a high selectivity for EA compared with other phenols which corresponded to high values of selectivity factor, demonstrating the selective affinity of MMIP towards EA.

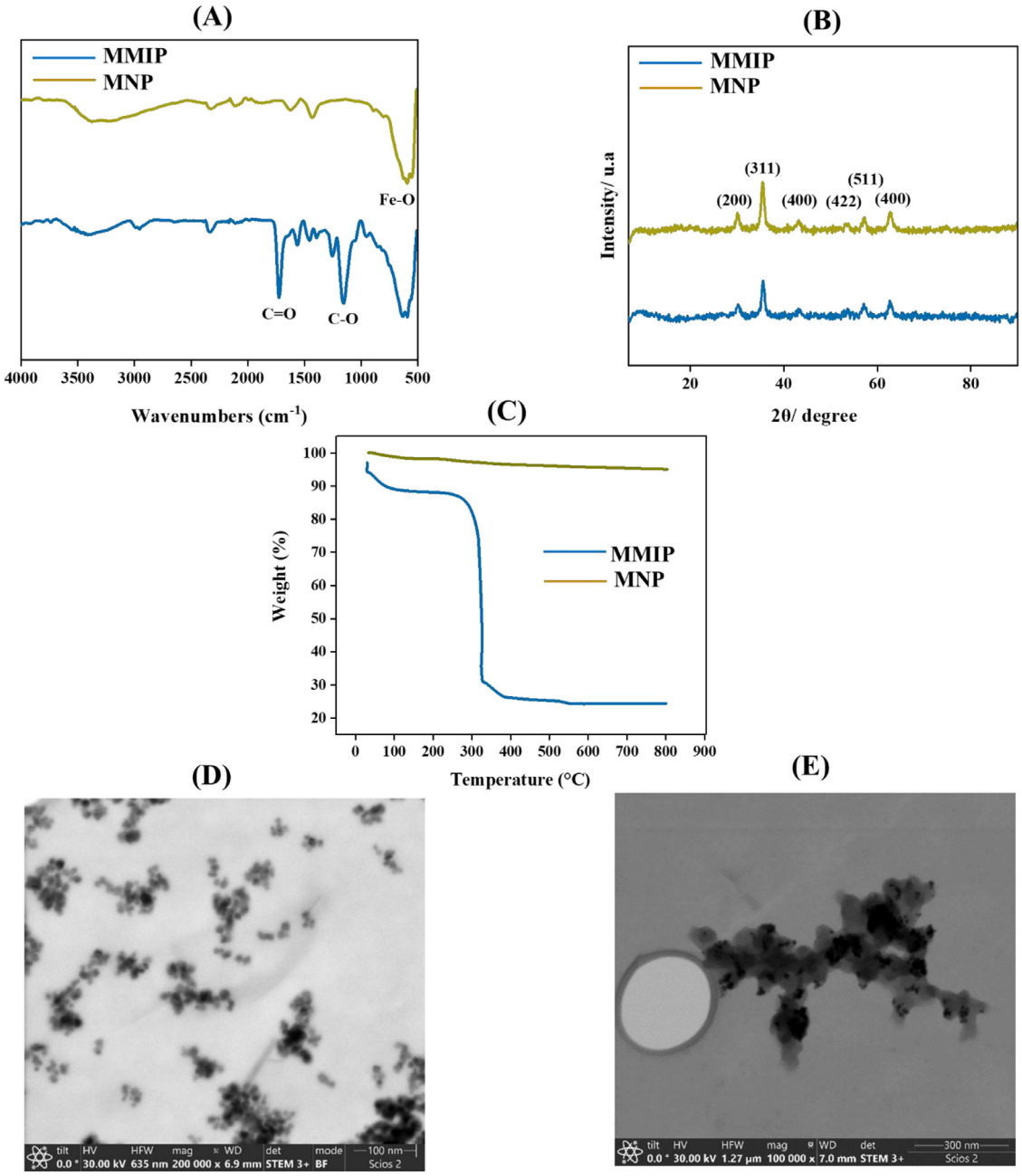

Fig. 2. (A) FT-IR spectra; (B) XRD diffractograms; (C) TGA curves (performed for MNP and MMIP); (D and E) Selected STEM images of MNP and MMIP, respectively.

3.6. SPE protocol

3.6.1. Effect of MMIP amount

The effect of this parameter on the SPE efficiency was evaluated by measuring the recoveries in terms of MMIP amounts, which ranged from 1 to 20 mg, with both the adsorption and elution time remaining fixed at 15 min. Fig. 4A showed the significant effect of the MMIP amount on the response, as confirmed by the ANOVA (as shown in **Table. S8A**), such that the recoveries progressively increased to reach an optimum value around 93% for 4 mg of MMIP. After that, they approximatively kept constant. Hence, the MMIP amount of 4 mg was chosen to be employed in the further experiments of SPE protocol, according to the pairwise Tukey comparison detailed in **Table. S8A,** which confirmed that there is no significant difference in recoveries when using a MMIP mass superior or equal to 4 mg.

3.6.2. Effect of adsorption time

Upon establishing the adequate MMIP amount, various adsorption time values were optimized in an interval ranging from 5 to 30 min (Fig. 4B). The calculated recoveries were increased significantly from 5 to 15 min, then they were kept in the steady-state. Hence, according to the statistical analysis (ANOVA and pairwise Tukey comparison), an adsorption time of 15 min was fixed in the SPE protocol as summarized in **Table. S8B**.

3.6.3. Effect of elution time

After determining the optimal MMIP amount and fixing the adsorption time on 15 min, elution time ranging from 5 to 60 min was evaluated. As shown in Fig. 4C and **Table. S8C**, the recoveries were noticeably increased accordingly to the elution time (as confirmed by ANOVA). After 15 min the recoveries were almost at the equilibrium state. Thus,

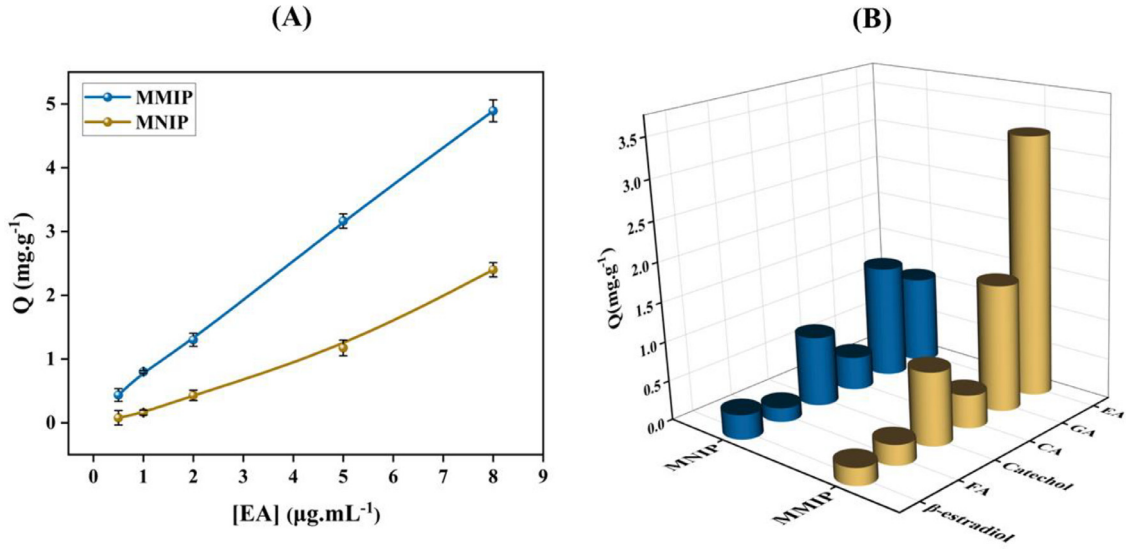

Fig. 3. (A) Isotherm assessment of MMIP and MNIP for different EA concentrations. (B) Selectivity study of the binding capacities for MNIP towards EA and several analogous molecules (GA, CA, Catechol, FA, and β-estradiol).

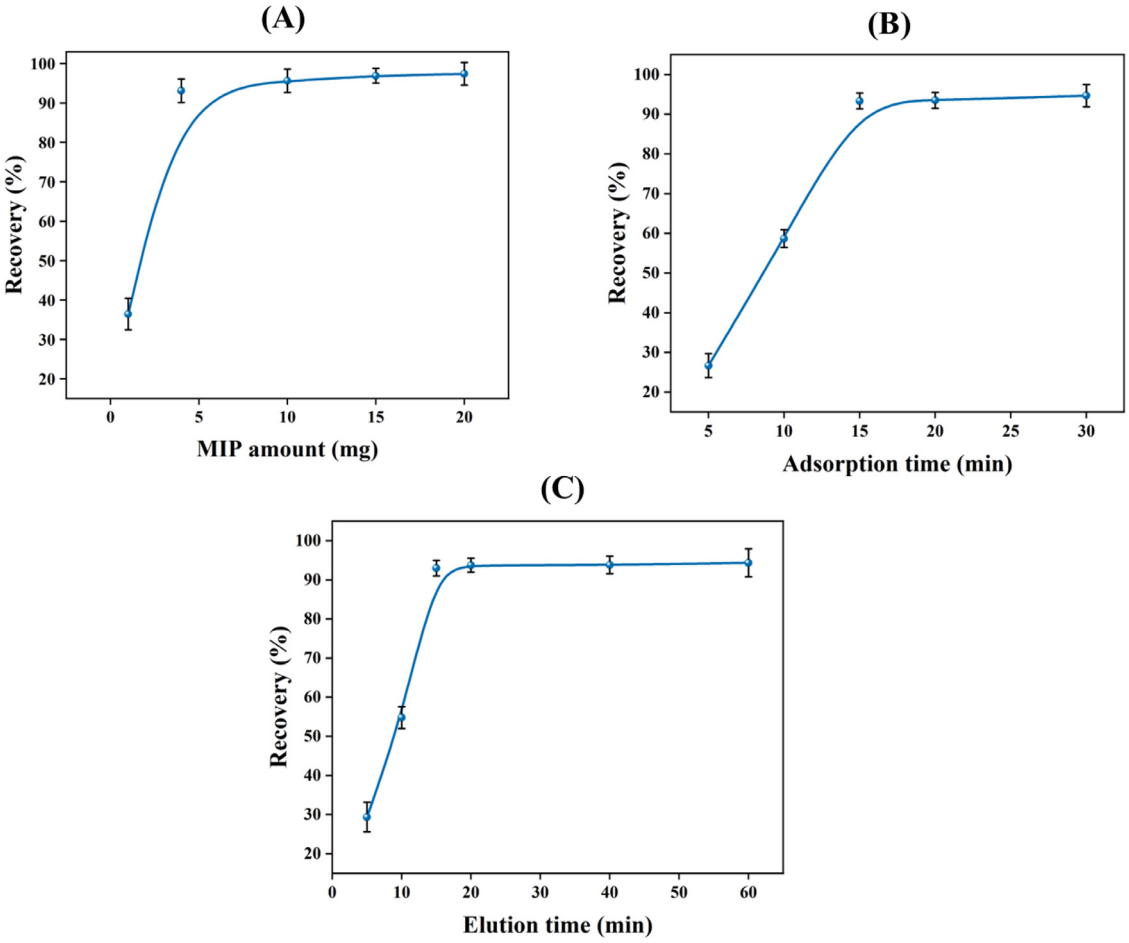

Fig. 4. Optimizations of SPE conditions: (A) MMIP amount; (B) elution time; and (C) adsorption time for 1 $\mu g{\cdot}mL^{-1}$ of EA.

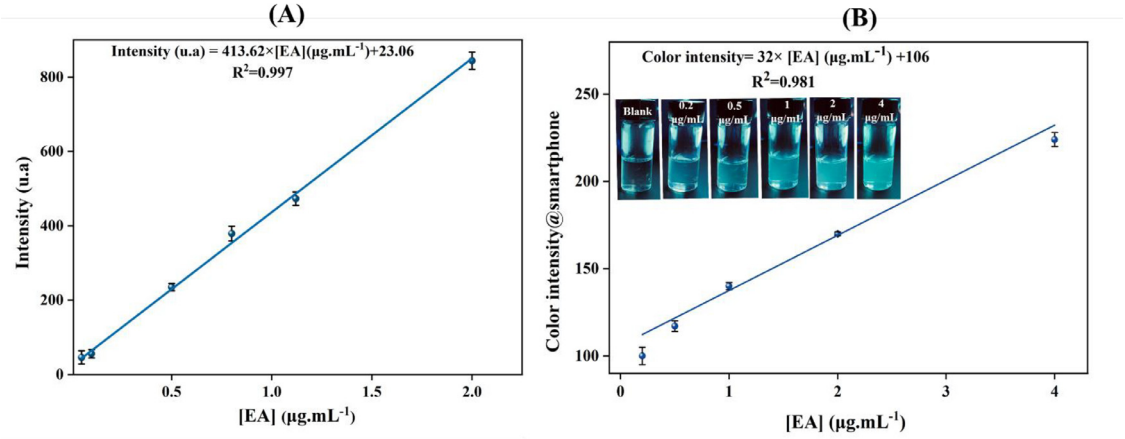

Fig. 5. (A) Calibration curve of the spectrofluorimetric detection of EA-borax; (B) Calibration curve of the smartphone-based fluorescence detection of EA using a hand-held UV lamp.

this time value was chosen after applying the pairwise Tukey comparison, which statistically proved that recoveries non-significantly varied for an elution time equal or superior to 15 min.

3.7. Fluorometric determination of EA

3.7.1. Spectrofluorometric detection

The interaction between EA and borax led to the formation of a complex with high fluorescence properties. This characteristic allowed the construction of a calibration curve by measuring the fluorometric intensities of this complex against various EA concentrations ranging from 0.05 to 2 $\mu g{\cdot}mL^{-1}$, as illustrated in Fig. 5A. Each experiment was measured in triplicate. According to the calibration curve, a linear regression equation of: $\text{Intensity (u.a)} = 413.62 \times [\text{EA}]\ (\mu g.mL^{-1}) + 23.06$ was obtained with a significant regression coefficient of 0.997 and a limit of detection and quantification of 0.007 and 0.02 $\mu g{\cdot}mL^{-1}$, respectively. These figures of merits were calculated from the calibration set using the following formula $LOQ = 3 \times LOD = \frac{10*SD}{Slope}$, where SD is the standard deviation of the blank. It is noteworthy that the fluorescence detection of EA-borax complex is sensitive, fast, and green.

3.7.2. Smartphone-based fluorescence detection

A novel approach for EA smartphone detection was applied in this work using a handheld UV lamp. Different concentrations of EA ranging from 0.2 to 4 $\mu g{\cdot}mL^{-1}$ were excited under the lamp at the excitation wavelength of 395 nm. The fluorescent colors were photographed with a smartphone (model iPhone XR with 1080p HD at 30 fps in resolution) to assess the RGB channels using the free ImageJ software.

As shown in **Fig. S4** the green channel is the most influential color in terms of EA concentrations. For this reason, this green intensity was chosen as the signal element for the construction of the calibration curve illustrated in Fig. 5B. The quantification and detection limits were 0.2 and 0.07 $\mu g{\cdot}mL^{-1}$, respectively.

The developed smartphone-based fluorescence method presented a large linear range. Since, it is not required to detect very small concentrations of EA in real samples, the developed smartphone diagnostic can be considered as an effective, rapid, and low-cost fluorescence sensor for the on-site visual detection of low and high EA concentrations.

3.8. Reusability study

The reusability of the developed MMIP was a major profit to evaluate the practical applications and the economic cost of the imprinting polymer. Effectively, numerous MMIP-SPE cycles were undertaken successively following the previously mentioned approach, yielding seven efficient recoveries ranging from 76 to 95% as shown in **Fig. S5**, which proved the durability and the cost-effectiveness of the developed MMIP.

3.9. Comparative study

Indeed, EA has a major importance. But, the synthesis of EA-MIP was difficult to accomplish. As a result, there are only a few works in the literature that successed in the formation EA imprinting polymers. However, the reported studies in Table 1 are still time consuming [52–54], complicated since they need fractionating columns [53], and they required toxic solvents [53,54]. As result, they were not considered environmentally friendly approaches for the EA determination. However, in the present work, the required time in the preparation of the MMIP, as well as the needed time in MMIP-SPE protocol was remarkably reduced. Moreover, the combination of MMIP-SPE with an immediate EA smartphone detection is used for the first time in the recent work. Thus, the novel developed approach demonstrated to be efficient, green, low-priced, and fast.

3.10. Real samples application

After determining the best MMIP-SPE protocol, it was used to investigate its real-world application and its reliability to detect EA in many natural samples, particularly grape, redberry, and green tea. The samples were spiked by 0.5 and 1 $\mu g{\cdot}mL^{-1}$ of EA. Indeed, the calculated recoveries were significantly important with values ranging from 83% to 102% when using the spectrofluorometer detection method and from

Table 1
Comparison study of the developed strategy with other published works using the imprinting polymers in SPE for EA extraction.

Adsorbent in SPE	Detection method	Binding time (h)	Recovery (%)	IF	Time (h)	Polymerization method	Ref
Nano MIP-SPE	UV-spectroscopy	1.5	86	3.8	3.5	Distillation-precipitation	[52]
MIP microspheres-SPE	HPLC	2	86	2.3	27	Distillation-precipitation	[53]
2D-MIP-SPE	HPLC	2	80–96	2–5	>24	Free-radical	[54]
This work	Fluorometry Smartphone	0.25	80–102	2.6–3.4	1h40min	Free-radical	–

Table 2
Extraction and detection of EA in grape, redberry, and green tea juices using the developed strategy MMIP-SPE coupled to the spectrofluorometer and smartphone-based fluorescence.

Sample	Conc. Before spiking ($\mu g \cdot mL^{-1}$)	Spiked. Conc ($\mu g \cdot mL^{-1}$)	Expected. Conc ($\mu g \cdot mL^{-1}$)	Spectrofluorometer			Smartphone-based fluorescence		
				Found. Conc ($\mu g \cdot mL^{-1}$)	Recovery (%)	RSD (%) ($n = 3$)	Found. Conc ($\mu g \cdot mL^{-1}$)	Recovery (%)	RSD (%) ($n = 3$)
Grape juice	0.25	0.50	0.75	0.69	88	1.30	0.65	80	2.07
		1.00	1.25	1.21	96	1.58	1.19	94	2.19
Redberry	1.60	0.50	2.10	2.05	90	1.85	2.00	80	2.79
juice		1.00	2.60	2.61	101	1.32	2.51	91	3.00
Green Tea	0.30	0.50	0.80	0.78	96	3.02	0.78	98	.2.12
		1.00	1.30	1.32	102	1.06	1.17	91	1.85

80% to 98% when using the proposed smartphone-based fluorescence detection method. Moreover, the relative standard deviations (RSDs) were noticeably inferior to 3% (as shown in Table 2), demonstrating that the developed MMIP-SPE revealed good precision and accuracy in EA extraction.

4. Conclusions

In the present paper, a new high-efficient MMIP for EA was prepared using a rapid and a green radical polymerization, which was assessed by a CCD to reveal the adequate conditions. The prepared MMIP exhibited high selectivity towards EA compared to several similar phenols with an imprinting factor around 3. Indeed, the MMIP was employed as a sorbent in the SPE for a selective, green, and rapid EA recognition. For EA detection, the proposed smartphone-based fluorescence method presented many advantages, including rapidity, cost-effectiveness, and on-site detection. Furthermore, the strategy of MMIP-SPE coupled to fluorescence presented a high accuracy and efficiency for EA extraction and determination in many fruit samples in which the experimental recoveries were ranging from 80% to 102% with low RSD (≥3%). Consequently, owing to the numerous features of the MMIPs, including the selectivity, rapidity, and reusability, MMIPs are the most promising sorbents to be used for the high-purification efficiency of polyphenols from plant matrices which will enhance the application of these valuable natural compounds in the pharmacy field. Furthermore, the application of smartphone-based fluorescence detection using UV lamp as the excitation source could be certainly of high importance for other purposes, particularly, in food control, environmental monitoring, and point of care sensing.

Declaration of Competing Interest

The authors declare that they have no known competing financial interests or personal relationships that could have appeared to influence the work reported in this paper.

Data availability

All data used are collected in the results included in the paper.

Acknowledgements

Ouarda El Hani and Abdelhafid Karrat gratefully acknowledge financial support from Erasmus+ KA107 (EU) Program of the University of Cádiz (Spain), through 'Servicio Español para la Internacionalización de la Educación' (SEPIE). Spanish authors acknowledge Junta de Andalucia (PAIDI) and the Institute of Research on Electron Microscopy and Materials (IMEYMAT) for providing research funds (NANO4(BIO)SENS project). Besides, we also thank Agencia Estatal de Investigación (AEI), Ministerio de Ciencia e Innovación of Spain, and FEDER funds (EU) for the "Multibioanalysis" research project (Proyecto de Generación del Conocimiento, PID2021–122578NB-I00) financed by MCIN/AEI/10.13039/501100011033 and by FEDER, UE "ERDF A way of making Europe". Authors thank 'Plan Propio 2022–2023' from University of Cadiz for their funding through the "Acceso al uso de Servicios Centrales de Investigación. Financiación de Actividades" program (Ref: SC2022–001).

Finally, the authors thank Electron Microscopy and X-Ray Diffraction and Fluorescence Divisions from Servicios Centrales de Investigación Científica y Tecnológica of University of Cadiz (SC-ICYT-UCA) for their technical assistance during SEM/STEM, EDS and XRD measurements, the TEP-243 research group for the help provided to register the FTIR spectra and Ms. María del Rocío González-Moya (Technician of the University of Cadiz, Spain) for her assistance in performing the TGA analyses.

Supplementary materials

Supplementary material associated with this article can be found, in the online version, at doi:10.1016/j.greeac.2023.100058.

References

[1] I.F. do Valle, H.G. Roweth, M.W. Malloy, S. Moco, D. Barron, E. Battinelli, J. Loscalzo, A.-.L. Barabási, Network medicine framework shows that proximity of polyphenol targets and disease proteins predicts therapeutic effects of polyphenols, Nat. Food 2 (2021) 143–155, doi:10.1038/s43016-021-00243-7.
[2] P. Sharma, Y.A. Hajam, R. Kumar, S. Rai, Complementary and alternative medicine for the treatment of diabetes and associated complications: a review on therapeutic role of polyphenols, Phytomed. Plus 2 (2022) 100188, doi:10.1016/j.phyplu.2021.100188.
[3] H. Rasouli, M.H. Farzaei, R. Khodarahmi, Polyphenols and their benefits: a review, Int. J. Food. Properties (2017) 1–42, doi:10.1080/10942912.2017.1354017.
[4] M. Hu, B. Wu, Z. Liu, Bioavailability of polyphenols and flavonoids in the era of precision medicine, Mol. Pharmac. 14 (2017) 2861–2863, doi:10.1021/acs.molpharmaceut.7b00545.
[5] W. Hao, H. Gan, L. Wang, J. Huang, J. Chen, Polyphenols in edible herbal medicine: targeting gut-brain interactions in depression-associated neuroinflammation, Crit. Rev. Food. Sci. Nutr (2022) 1–17, doi:10.1080/10408398.2022.2099808.
[6] A. Aguilera-Carbo, C. Augur, L. Prado-Barragan, C. Aguilar, E. Favela-Torres, Extraction and analysis of ellagic acid from novel complex sources, Chemical. Papers 62 (2008), doi:10.2478/s11696-008-0042-y.
[7] Q. Cui, R. Du, M. Anantpadma, A. Schafer, L. Hou, J. Tian, R. Davey, H. Cheng, L. Rong, Identification of ellagic acid from plant rhodiola rosea L. as an Anti-Ebola Virus Entry Inhibitor, Viruses 10 (2018) 152, doi:10.3390/v10040152.
[8] J. Sharifi-Rad, C. Quispe, C.M.S. Castillo, R. Caroca, M.A. Lazo-Vélez, H. Antonyak, A. Polishchuk, R. Lysiuk, P. Oliinyk, L. De Masi, P. Bontempo, M. Martorell, S.D. Daştan, D. Rigano, M. Wink, W.C. Cho, Ellagic acid: a review on its natural sources, chemical stability, and therapeutic potential, Oxid. Med. Cell. Longev 2022 (2022) 1–24, doi:10.1155/2022/3848084.
[9] J. Zhao, J. Liu, F. Wang, S. Wang, H. Feng, X. Xie, F. Hao, L. Zhang, C. Fang, Volatile constituents and ellagic acid formation in strawberry fruits of selected cultivars, Food. Research. International 138 (2020) 109767, doi:10.1016/j.foodres.2020.109767.
[10] J.-.L. Ríos, R. Giner, M. Marín, M. Recio, A pharmacological update of ellagic acid, Planta. Med 84 (2018) 1068–1093, doi:10.1055/a-0633-9492.
[11] S. Ding, H. Jiang, J. Fang, Regulation of immune function by polyphenols, J. Immunol. Res 2018 (2018) 1–8, doi:10.1155/2018/1264074.
[12] Y. Wei, G. Zhu, C. Zheng, J. Li, S. Sheng, D. Li, G. Wang, F. Zhang, Ellagic acid protects dopamine neurons from rotenone-induced neurotoxicity via activation of Nrf2 signalling, J. Cell. Mol. Med 24 (2020) 9446–9456, doi:10.1111/jcmm.15616.
[13] Z. Mansouri, M. Dianat, M. Radan, M. Badavi, Ellagic acid ameliorates lung inflammation and heart oxidative stress in elastase-induced emphysema model in rat, Inflammation 43 (2020) 1143–1156, doi:10.1007/s10753-020-01201-4.

[14] A. Gupta, A.K. Singh, R. Kumar, S. Jamieson, A.K. Pandey, A. Bishayee, Neuroprotective potential of ellagic acid: a critical review, Adv. Nutr. 12 (2021) 1211–1238, doi:10.1093/advances/nmab007.

[15] Y. Farbood, M. Rashno, S. Ghaderi, S.E. Khoshnam, A. Sarkaki, K. Rashidi, M. Rashno, M. Badavi, Ellagic acid protects against diabetes-associated behavioral deficits in rats: possible involved mechanisms, Life. Sci. 225 (2019) 8–19, doi:10.1016/j.lfs.2019.03.078.

[16] N.A. Afifi, M.A. Ibrahim, M.K. Galal, Hepatoprotective influence of quercetin and ellagic acid on thioacetamide-induced hepatotoxicity in rats, Can, J. Physiol. Pharmacol. 96 (2018) 624–629, doi:10.1139/cjpp-2017-0651.

[17] T. Morikawa, K. Imura, Y. Akagi, O. Muraoka, K. Ninomiya, Ellagic acid glycosides with hepatoprotective activity from traditional Tibetan medicine Potentilla anserina, J. Nat. Med 72 (2018) 317–325, doi:10.1007/s11418-017-1137-y.

[18] M. Saadullah, M. Asif, A. Sattar, K. Rehman, S. Shah, M. Saleem, A. Shah, M. Wajid, A. Rasool, M. Uzair, S. Afzal, K. Afzal, Cytotoxic and antioxidant potentials of ellagic acid derivatives from *Conocarpus lancifolius* (Combretaceae), Trop. J. Pharm. Res. 19 (2020) 1037–1080, doi:10.4314/tjpr.v19i5.24.

[19] V. Baradaran Rahimi, M. Ghadiri, M. Ramezani, V.R. Askari, Antiinflammatory and anti-cancer activities of pomegranate and its constituent, ellagic acid: evidence from cellular, animal, and clinical studies, Phytother. Res 34 (2020) 685–720, doi:10.1002/ptr.6565.

[20] P. Gupta, T. Mohammad, P. Khan, M.F. Alajmi, A. Hussain, Md.T. Rehman, Md.I. Hassan, Evaluation of ellagic acid as an inhibitor of sphingosine kinase 1: a targeted approach towards anticancer therapy, Biomed. Pharmacother 118 (2019) 109245, doi:10.1016/j.biopha.2019.109245.

[21] A. Sridhar, M. Ponnuchamy, P.S. Kumar, A. Kapoor, D.-V.N. Vo, S. Prabhakar, Techniques and modeling of polyphenol extraction from food: a review, Environ. Chem. Lett 19 (2021) 3409–3443, doi:10.1007/s10311-021-01217-8.

[22] F. Al Juhaimi, M.M. Özcan, K. Ghafoor, E.E. Babiker, S. Hussain, Comparison of cold-pressing and soxhlet extraction systems for bioactive compounds, antioxidant properties, polyphenols, fatty acids and tocopherols in eight nut oils, J. Food. Sci. Technol 55 (2018) 3163–3173, doi:10.1007/s13197-018-3244-5.

[23] P. Panichayupakaranant, A. Itsuriya, A. Sirikatitham, Preparation method and stability of ellagic acid-rich pomegranate fruit peel extract, Pharm. Biol 48 (2010) 201–205, doi:10.3109/13880200903078503.

[24] L. Wang, B. Lian, W. Wu, Y. Deng, Y. Liu, L. Wang, Y. Li, Z. Wang, X. Zhao, Optimization of ellagic acid purification from pomegranate husk by antisolvent recrystallization, Chem. Eng. Technol. 41 (2018) 1188–1198, doi:10.1002/ceat.201700301.

[25] T. Jaipetch, S. Hongthong, S. Bunteang, R. Akkarawongsapat, J. Limthongkul, C. Napaswad, K. Suksen, N. Nuntasaen, V. Reutrakul, C. Kuhakarn, A New Ellagic Acid From the Leaves and Twigs of *Irvingia malayana*, Nat. Prod. Commun 14 (2019) 1934578X1984816, doi:10.1177/1934578X19848164.

[26] A. Spisso, F.J.V. Gomez, M.Fernanda Silva, Determination of ellagic acid by capillary electrophoresis in Argentinian wines, Electrophoresis 39 (2018) 1621–1627, doi:10.1002/elps.201700487.

[27] A. Masci, A. Coccia, E. Lendaro, L. Mosca, P. Paolicelli, S. Cesa, Evaluation of different extraction methods from pomegranate whole fruit or peels and the antioxidant and antiproliferative activity of the polyphenolic fraction, Food. Chem 202 (2016) 59–69, doi:10.1016/j.foodchem.2016.01.106.

[28] R. Pallavi, S. Jha, A validated quantification of gallic acid and ellagic acid in Triphala using a high-performance thin-layer chromatography method, JPC-J. Planar. Chromat 34 (2021) 447–453, doi:10.1007/s00764-021-00130-8.

[29] R. Agregán, P.E.S. Munekata, X. Feng, G. Astray, B. Gullón, J.M. Lorenzo, Recent advances in the extraction of polyphenols from eggplant and their application in foods, LWT 146 (2021) 111381, doi:10.1016/j.lwt.2021.111381.

[30] Y. Oualcadi, M.F. Sebban, F. Berrekhis, Improvement of microwave-assisted Soxhlet extraction of bioactive compounds applied to pomegranate peels, J. Food. Process. Preserv 44 (2020), doi:10.1111/jfpp.14409.

[31] B.R. Albuquerque, S.A. Heleno, M.B.P.P. Oliveira, L. Barros, I.C.F.R. Ferreira, Phenolic compounds: current industrial applications, limitations and future challenges, Food. Funct 12 (2021) 14–29, doi:10.1039/D0FO02324H.

[32] N.P. Kelly, A.L. Kelly, J.A. O'Mahony, Strategies for enrichment and purification of polyphenols from fruit-based materials, Trends Food Sci. Technol 83 (2019) 248–258, doi:10.1016/j.tifs.2018.11.010.

[33] M. Musa, W.A. Wan Ibrahim, F. Mohd Marsin, A.S. Abdul Keyon, H. Rashidi Nodeh, Graphene-magnetite as adsorbent for magnetic solid phase extraction of 4-hydroxybenzoic acid and 3,4-dihydroxybenzoic acid in stingless bee honey, Food. Chem 265 (2018) 165–172, doi:10.1016/j.foodchem.2018.04.020.

[34] L. Karadurmus, S. Bilge, A. Sınağ, S.A. Ozkan, Molecularly imprinted polymer (MIP)-Based sensing for detection of explosives: current perspectives and future applications, TrAC. Trends. Analy. Chem. 155 (2022) 116694, doi:10.1016/j.trac.2022.116694.

[35] A. Karrat, J.M. Palacios-Santander, A. Amine, L. Cubillana-Aguilera, A novel magnetic molecularly imprinted polymer for selective extraction and determination of quercetin in plant samples, Anal. Chim. Acta 1203 (2022) 339709, doi:10.1016/j.aca.2022.339709.

[36] K. Karim, A. Lamaoui, A. Amine, Acetazolamide smartphone-based detection via its competition with sulfamethoxazole on molecularly imprinted polymer: a proof-of-concept, J. Pharm. Biomed. Anal 219 (2022) 114954, doi:10.1016/j.jpba.2022.114954.

[37] M. Arabi, A. Ostovan, A.R. Bagheri, X. Guo, L. Wang, J. Li, X. Wang, B. Li, L. Chen, Strategies of molecular imprinting-based solid-phase extraction prior to chromatographic analysis, TrAC. Trends. Analy. Chem 128 (2020) 115923, doi:10.1016/j.trac.2020.115923.

[38] D. Elfadil, F. Della Pelle, D. Compagnone, A. Amine, Green Synthesis of Molecularly Imprinted Polymers for Dispersive Magnetic Solid-Phase Extraction of Erythrosine B Associated with Smartphone Detection in Food Samples, Materials. (Basel) 15 (2022) 7653, doi:10.3390/ma15217653.

[39] Y. Cao, T. Feng, J. Xu, C. Xue, Recent advances of molecularly imprinted polymer-based sensors in the detection of food safety hazard factors, Biosen. Bioelect. 141 (2019) 111447, doi:10.1016/j.bios.2019.111447.

[40] O. El Hani, A. Karrat, K. Digua, A. Amine, Advanced molecularly imprinted polymer-based paper analytical device for selective and sensitive detection of Bisphenol-A in water samples, Microchem. J. (2022) 108157, doi:10.1016/j.microc.2022.108157.

[41] M. Dinc, C. Esen, B. Mizaikoff, Recent advances on core–shell magnetic molecularly imprinted polymers for biomacromolecules, TrAC. Trends. Analy. Chem. 114 (2019) 202–217, doi:10.1016/j.trac.2019.03.008.

[42] A. Karrat, A. Amine, Solid-phase extraction combined with a spectrophotometric method for determination of Bisphenol-A in water samples using magnetic molecularly imprinted polymer, Microchem. J. 168 (2021) 106496, doi:10.1016/j.microc.2021.106496.

[43] L. Sepúlveda, J.E. Wong-Paz, J. Buenrostro-Figueroa, J.A. Ascacio-Valdés, A. Aguilera-Carbó, C.N. Aguilar, Solid state fermentation of pomegranate husk: recovery of ellagic acid by SEC and identification of ellagitannins by HPLC/ESI/MS, Food. Biosci 22 (2018) 99–104, doi:10.1016/j.fbio.2018.01.006.

[44] A. Szmagara, A. Krzyszczak, I. Sadok, K. Karczmarz, M.M. Staniszewska, E.A. Stefaniak, Determination of ellagic acid in rose matrix by spectrofluorimetry, J. Food. Comp. Analy. 78 (2019) 91–100, doi:10.1016/j.jfca.2019.02.003.

[45] J. Sádecká, J. Tóthová, Spectrofluorimetric determination of ellagic acid in brandy, Food. Chem 135 (2012) 893–897, doi:10.1016/j.foodchem.2012.06.019.

[46] G. Rateni, P. Dario, F. Cavallo, Smartphone-based food diagnostic technologies: a Review, Sensors 17 (2017) 1453, doi:10.3390/s17061453.

[47] A. Atayat, L. Mergola, N. Mzoughi, R. Del Sole, Response surface methodology approach for the preparation of a molecularly imprinted polymer for solid-phase extraction of fenoxycarb pesticide in mussels, J. Sep. Sci. 42 (2019) 3023–3032, doi:10.1002/jssc.201900344.

[48] O. El hani, A. Karrat, K. Digua, A. Amine, Development of a simplified spectrophotometric method for nitrite determination in water samples, Mole. Biomole. Spectr. 267 (2022) 120574, doi:10.1016/j.saa.2021.120574.

[49] N. Ben Messaoud, A. Ait Lahcen, C. Dridi, A. Amine, Ultrasound assisted magnetic imprinted polymer combined sensor based on carbon black and gold nanoparticles for selective and sensitive electrochemical detection of Bisphenol A, Chemical 276 (2018) 304–312, doi:10.1016/j.snb.2018.08.092.

[50] F. Pena-Pereira, W. Wojnowski, M. Tobiszewski, AGREE—analytical GREEnness metric approach and software, Anal. Chem. 92 (2020) 10076–10082, doi:10.1021/acs.analchem.0c01887.

[51] V. Mazzaracchio, A. Sassolini, K.Y. Mitra, D. Mitra, G.M. Stojanović, A. Willert, E. Sowade, R.R. Baumann, R. Zichner, D. Moscone, F. Arduini, A fully-printed electrochemical platform for assisted colorimetric detection of phosphate in saliva: greenness and whiteness quantification by the AGREE and RGB tools, Green. Analy. Chem. 1 (2022) 100006, doi:10.1016/j.greeac.2022.100006.

[52] N. Yucel, H. Gulen, P.Cakir Hatir, Molecularly imprinted polymer nanoparticles for the recognition of ellagic acid, J. Appl. Polymer. Sci 139 (2022), doi:10.1002/app.52952.

[53] H. Zhang, S. Zhao, L. Zhang, B. Han, X. Yao, W. Chen, Y. Hu, Preparation of ellagic acid molecularly imprinted polymeric microspheres based on distillation-precipitation polymerization for the efficient purification of a crude extract: liquid Chromatography, J. Sep. Science. 39 (2016) 3098–3104, doi:10.1002/jssc.201600355.

[54] G. Sun, Y. Liu, H. Ahat, A. Shen, X. Liang, X. Xue, Y. Luo, J. Yang, Z.-.S. Liu, H.A. Aisa, Two-dimensional" molecularly imprinted solid-phase extraction coupled with crystallization and high performance liquid chromatography for fast semi-preparative purification of tannins from pomegranate husk extract, J. Chromatogr. A 1505 (2017) 35–42, doi:10.1016/j.chroma.2017.05.033.